SLAC-PUB-10214

Sizing of Microdrops

Irwin T. Lee, Sewan Fan, Valerie Halyo, Peter C. Kim,
Eric R. Lee, Martin L. Perl and Howard Rogers
Stanford Linear Accelerator Center
2575 Sand Hill Road, Menlo Park, CA, 94025

March 26, 2003

Abstract

Several techniques for determining the size of small fluid microdrops with diameter ranging from 5 μm to 30 μm have been developed and evaluated using an automated variation on the Millikan oil drop experiment. The average diameter of a large sample of monodisperse fluid drops was determined by measuring their terminal velocity in air, or if charged, their motion under the influence of an electric field, as well as by measurement of the magnitude of their Brownian motion. The diameter of individual drops was determined optically, by direct observation using an imaging system based on a coupled device (CCD) camera. The technique used to analyze the image data is based on a best fit technique taking the point spread function (PSF) of the lens into account, and yields results accurate to 1% (based on a single image) without the need for any calibration. By combining this technique with terminal velocity measurements, the density of the fluid can be determined to similar accuracy.

Work supported in part by the Department of Energy contract DE-AC03-76SF00515.

Contributed to the 2003 Particle Accelerator Conference 2003,
5/12/2003 - 5/16/2003, Portland, OR, USA

1 Introduction

We have built an automated variation of the Millikan oil drop experiment for the purpose of conducting a search for elementary particles with fractional charge. This apparatus has been used to study a sample of 1.7×10^7 drops of silicone oil (approximately 70.1 mg), and is described in detail in [1], as well as in [2], which describes a previous run, collecting data corresponding to 17.4 mg total throughput. In the course of the analysis of this experimental data, it was necessary to develop various techniques for determining the size of these microdrops, both using image analysis techniques and from their trajectories through the apparatus. The microdrops ranged from 5 to 30 μm in diameter.

In Section 2 we describe the apparatus used for producing the microdrops of a specific size and for measuring their properties. In Section 3 we describe our use of the well known technique of determining the drop diameter from the terminal velocity of the drop falling in air under gravity. In Section 4 we show how the terminal velocity of a *charged* microdrop in an electric field can be used to determine drop diameter. Section 5 describes a less known method for measuring drop diameter using Brownian motion. Finally in Section 6 we discuss direct optical measurement of drop diameter using a lens and CCD camera system.

2 Apparatus and Microdrop Production

Our microdrops are produced by a piezoelectrically actuated, drop-on-demand ejector developed from inkjet print head technology. This technology allows

the controlled production of drops with sizes ranging from 5 μm to 50 μm, depending on orifice size and the parameters of the pulses used to drive the piezoelectric actuator. Once set for a specific drop size, drops can be produced with a dispersion in size on the order of 0.1%. A detailed exposition of the necessary technology and practical techniques is given in [3].

The drops fall through a temperature and convection controlled measurement chamber, where they are acted on by an electric field. Temperature gradients in similar chambers from previous apparatus were found to be less than $0.1^{\circ}K$, which was below the sensitivity of the instruments used. The microdrops themselves are an excellent probe for convection— since their trajectories do not show measurable deflections, the convection velocities in the chamber are known to be significantly less than ≈ 10 μm/s. The electric field, which alternates with a frequency of 2.5 Hz, causes the drops to oscillate in the horizontal direction. The electric field, produced by parallel capacitor plates, has a strength which is limited by breakdown of the air to approximately 1.8 MV/m. A drop with 20 μm diameter has a terminal velocity due to gravity of 10.6 mm/s, and a terminal velocity due to the electric field of 83 μm/s per electron charge. The apparatus also allows for the optional use of an upwards laminar airflow in the measurement chamber, such that the downwards velocity of the drops can be decreased to approximately 1 mm/s.

As the drops fall through the measurement region, their trajectories are observed and measured. The imaging system consists of a monochrome CCD camera, Cohu model 4110, whose active sensor area is 6.4 mm by 4.8 mm, divided into an array of 739 by 484 picture elements (pixels) respectively.

Each pixel is therefore 8.7 μm by 20. μm. A Bitflow Data Raptor framegrabber connected to the digital output lines of the camera reads these pixels out at 8 bit resolution, producing a greyscale value ranging from 0–255. Because of interlacing and details relating to the framegrabber, images of 736 by 240 pixels are acquired, where the reduction in the number of rows is due to binning of adjacent rows. Using a carefully controlled illumination source, the output was shown to be linear with respect to the source intensity. The noise levels in each pixel were measured to be uniform across the CCD surface, and independent of the illumination level, at the levels at which the CCD was operated. These fluctuations were Gaussian distributed with a sigma of 1.3 greyscale units.

The camera and a 135 mm focal length, $f/11$ photographic enlarging lens are mounted on an optical rail such that they are coaxial, with a fixed separation of 413 mm. This arrangement causes objects 201 mm in front of the lens to be imaged onto the surface of the CCD, at a magnification of 2.06×. This arrangement causes the image of a 20 μm microdrop to extend over approximately 5 pixels by 2 pixels.

Illumination is provided by a bank of light emitting diodes (LEDs), 370 mm in front of the lens, which are diffused by a ground glass screen. The LEDs are strobed at 10 Hz, with pulse widths on the order of a few tens of microseconds. These pulse widths are short enough such that they do not measurably smear the drop images, since the distance traveled by the drop during this time is small compared to its size. Due to the geometry of the apparatus, it was not possible to achieve perfectly uniform illumination across the entire field of view. For this reason, background calibrations were

taken using the intended illumination levels with nothing in the focal plane. This background level was removed from the raw data by subtraction,

As oil droplets fall through the field of view of the system, they appear as dark shadows on a bright background. A typical image is shown in Figure 1.

[Figure 1 about here.]

3 Terminal Velocity

A sphere moving in a viscous medium experiences a drag force given by Stokes's Law,

$$F = 6\pi\eta r v \tag{1}$$

where η is the coefficient of viscosity of the air, r is the radius of the drop, and v is its velocity.

If the density is known, then the radius can directly be calculated from the terminal velocity of the drop under gravity (v_g).

$$r = \sqrt{\frac{9}{2}\frac{v_g \eta}{\rho g}} \tag{2}$$

Using the apparatus described, a 20 μm diameter drop is observed for 0.2 s as it falls through the measurement region. Under such conditions, the precision in the measured terminal velocity is approximately 0.05%, yielding an error on the radius of 0.025%. The precision is limited primarily by random fluctuations introduced by Brownian motion, which is intrinsic to the method and cannot be reduced. The absolute accuracy is also limited

by the uncertainty in the density ρ of the fluid, as well as the accuracy to which the viscosity η is known.

It is possible to increase the precision of this terminal velocity measurement by using an upwards laminar airflow. The effect of this airflow is to increase the time under which the drop is observed, which reduces the relative contribution of Brownian motion. Increases in precision of up to a factor of 3 have been achieved, by increasing the observation time by a factor of 10. A significant drawback of using laminar airflow is that the absolute precision of the terminal velocity measurement becomes limited by the accuracy to which the airflow velocity and any inhomogeneities in the velocity are known.

4 Quantized charge peaks

Under the influence of an electric field E, a drop with charge q reaches a terminal velocity (v_e) again given by Stokes's Law.

$$v_e = \frac{E}{6\pi\eta r} q \tag{3}$$

Since electric charge is quantized in units of the electron charge e, a large sample of monodisperse drops will show a distribution of v_e with sharp peaks separated by $eE/6\pi\eta r$, as shown in Figure 2. From the measured separation of 0.077 mm/s between adjacent peaks, it is possible to calculate the average drop radius to be 21.5 μm in the data sample.

[Figure 2 about here.]

The width of the observed v_e peaks is primarily due to Brownian motion and position measurement accuracy of the microdrops. However, there is a contribution due to the dispersion of the drop size in the sample. This contribution is relatively small since the dispersion was small.

$$v_{e,measured} = \frac{E}{6\pi\eta}\frac{1}{r}q + \Delta v_{Brownian} + \Delta v_{positionaccuracy} \tag{4}$$

While the term involving the Brownian motion and measurement error do not depend on the charge, the contribution from the term involving r increases as the charge of the drop increases. Since these terms contribute in quadrature, eventually the width increases with q^2. A measurement of the increase in the width of the observed peak as a function of the charge can then be used to extract the dispersion in the drop size present in the sample. From the data shown in Figure 3, the dispersion in drop size can be calculated to be 0.1%. Note that this method can be applied without a quantitative understanding of Brownian motion and the position measurement accuracy, and in addition is independent of the density of the fluid.

[Figure 3 about here.]

5 Brownian motion

A microdrop in air undergoes random Brownian motion characterized by the diffusion constant D:

$$< x^2 >= 2D\Delta t, D = \frac{kT}{6\pi\eta r} \tag{5}$$

Here k is the Boltzmann constant, T is the absolute temperature, r is the drop radius, and Δt is the time interval under which the drop is under observation. It is possible to perform a direct measurement of Brownian motion, even when there is significant error in the individual position measurements (centroiding error), since these random contributions have different statistical properties.

Consider the sequence of position measurements x_i of the trajectory of a drop. For two consecutive measurements, j and $j-1$, the velocity measurement $v_{x,j}$ is given by

$$v_{x,j} \equiv \frac{x_j - x_{j-1}}{\Delta t}. \tag{6}$$

Here, Δt is the time between successive frames, 0.1 s in our case. Since Δt is known with very good precision, the error in measuring v_x comes from the error in determining the x_i of the drop centers, and from Brownian motion. Take the error in centroiding to be normally distributed with a standard deviation of σ_c.

During the time Δt between any two successive measurements of the x_i positions, Brownian motion adds a random contribution with standard deviation given by Eq. (5).

The trajectory of a drop can thus be written as

$$\begin{aligned} x_j &= x_0 + \sigma_{c,j} + \sum_{i=2}^{j} \sigma_{b,i} \\ j &= 1, 2, \ldots, N_{measurements} \end{aligned} \tag{7}$$

with x_0 set by the initial position of the drop, and where the $\sigma_{c,i}$ ($\sigma_{b,i}$) are a sequence of random numbers representing the random contribution of measurement errors (Brownian motion), and are normally distributed with a std. dev. of σ_c (σ_b).

It then follows that

$$v_{x,j}\Delta t = \sigma_{b,j} + \sigma_{c,j} - \sigma_{c,j-1} \tag{8}$$

and

$$\langle v_{x,j} v_{x,k} \rangle \, \Delta t^2 = \begin{cases} 2\sigma_c^2 + \sigma_b^2, & j = k \\ -\sigma_c^2, & |j-k| = 1 \\ 0, & \text{otherwise.} \end{cases} \tag{9}$$

Therefore the total error on any given velocity measurement, σ_v, is given by $\sigma_v^2 = 2\sigma_c^2 + \sigma_b^2$, and the centroiding error introduces an anti-correlation with magnitude $-\sigma_c^2$ in two consecutive velocity measurements, due to the shared position measurement. We use the concept summarized in Eq. (9) and the observed distributions of the $v_{x,i}$ to separate σ_c from σ_b.

[Figure 4 about here.]

We illustrate this method by applying it to the data obtained in our recent fractional charge experiment [1], where we find

$$\sigma_c = 0.31 \ \mu\text{m}, \ \sigma_b = 0.47 \ \mu\text{m}, \tag{10}$$

in the measurement region. Compared to the size of an individual pixel on the CCD, the centroiding error is small, approximately 1/30 of a pixel.

Since the magnitude of the Brownian motion, given by Eq. (5), does not depend on the mass or charge of the drop, the value of σ_b obtained provides an independent check on the size of the drops, and is consistent with the 21.5 μm size determined from the gravitational terminal velocity and the electric field terminal velocity.

Since this measurement requires a large ensemble of monodisperse drops, it can only be used to determine the average radius of the ensemble, with the precision of this measurement depending on the size of the data sample as well as the spread in the drop size.

6 Optical Sizing

6.1 Theoretical Model

We use the approximation that the intensity distribution $I(x, y)$, (with increasing I being darker), observed at the surface of the CCD due to a microdrop of radius r is the circular shadow expected from geometric optics, convolved with a gaussian point spread function (PSF). This approximation is commonly used, for example see [4].

$$I_{geometric}(x,y) = \begin{cases} 0, & \sqrt{(x-x_0)^2+(y-y_0)^2} > r \\ 1, & \sqrt{(x-x_0)^2+(y-y_0)^2} \leq r \end{cases} \quad (11)$$

$$I_{PSF}(x,y) = \frac{1}{2\pi}\frac{A}{\sigma^2}e^{-\frac{x^2+y^2}{2\sigma^2}} \quad (12)$$

$$I = I_{geometric} * I_{PSF} \quad (13)$$

$$= \int\int I_{geometric}(x',y')I_{PSF}(x'-x, y'-y)dx'dy' \quad (14)$$

This model is a non-linear function of 5 parameters, x_0, y_0, r, A, and σ. In the above, x_0 and y_0 represent the position of the image of the microdrop on the CCD, while r is its apparent radius. For drops which are in the focal plane, the point spread function characterized by its width σ and amplitude A, is primarily due to diffraction caused by the finite aperture size of the lens. Of course, other non-idealities in the optical system will inevitably contribute as well. In addition, we approximate that small deviations from perfect focus of the object increase the width of this function.

Combining a direct calculation of the convolution, and using standard numerical methods for minimization, it is possible to find the best (minimized χ^2) fit parameters for the observed image of any given drop.

6.2 Calibration of Optical System

Since σ and A are properties of the optical system, it is possible to measure these quantities by observing known objects which are well characterized. The resultant best fit to σ and A can then be taken to be known, which reduces the complexity of the model (Eq. (14)) to 3 parameters.

The optical calibration target used was a chrome on glass mask, with simulated drops (circular spots) of 12.0 μm, 17.0 μm, 24.0 μm, and 33.9 μm, with an uncertainty of 0.3μm. Given the parameters of the imaging system, this is a difficult range since the observed images transition from an apparently Gaussian image at 12.0 μm to the profile of the 33.9 μm spot which clearly has a flat plateau.

Based on a large number of images of these spots, σ and A were determined, with σ measured to be 1.1 pixels, which is roughly what one would

expect from diffraction. As a check, these measurements were repeated with the calibration target slightly out of focus. As expected, σ was found to increase and A to decrease, with no significant effect on the measured r.

Given σ and A, it is possible to calibrate the measured value of r to the actual drop size, as shown in Figure 5. It is evident from the uncertainties that the model is less accurate for smaller drop sizes.

[Figure 5 about here.]

The data show quantitative agreement of the best fit r parameter with the actual drop size, and indicate a measurement accuracy of 1%. If we are able to make multiple measurements of the same drop, as is the case in the fractional charge work, the sizing accuracy can be improved either by averaging the measurements, or by combining the centroid data entering the fit.

6.3 Microdrop data

In order to quantitatively check the performance of this technique on drops, several different sizes of microdrops were produced and measured in the apparatus, with no airflow used. Two different fluids, Dow Corning 200 5 cs silicone oil and Ultra Chemical Ultraol 50NF white mineral oil were used. By Stokes's Law the terminal velocity due to gravity is proportional to r^2, as shown in Eq. (2), where the constant depends on ρ. The data for the two fluids are shown in Figure 6. From the measured slopes, the densities can be calculated to be 0.94±0.02 g/cc for silicone oil, and 0.78±0.02 g/cc for

Ultraol. A direct volumetric measurement of the densities of the samples yielded 0.91 g/cc for silicone oil and 0.78 g/cc for Ultraol[5].

[Figure 6 about here.]

7 Discussion

Given a fluid of known density, and in the absence of airflow, the well known terminal velocity measurement described in Section 3 gives the best absolute measurement of drop size. Brownian motion measurements and charge peak measurements are also useful for characterizing the average size of a large sample of drops, if they are approximately monodisperse.

The fractional charge search is designed to accurately measure the charge of a very large number ($\approx 10^7$) of individual microdrops, and detect single anomalous events. Since the sample material to be tested is a suspension of finely ground meteorite, it is necessary to prevent density (and hence mass) variations from causing drops to appear fractionally charged. For this reason, it was necessary to develop a technique to size microdrops, independently of their mass. It was not clear from the literature how well an optical technique would work, given the constraints that the images would only contain a small number of pixels, and since diffraction would be significant. Using a pure fluid in our apparatus allowed us to validate these optical techniques by comparison with terminal velocity measurements. The precision that was achieved was encouraging. Also interesting was that the technique does not have any free parameters, in that no calibration from data was necessary. Because of this, the method is generally applicable to

finding the density of unknown fluids, particularly useful if the available sample size is small. Since the density of individual microdrops with volumes on the order of picoliters can be measured to accuracies of 1%, larger volumes can be measured to significantly better accuracies.

Acknowledgment

Work supported by Department of Energy contract DE-AC03-76SF00515.

References

[1] I. T. Lee *et al.*, Phys. Rev. D **66**, 012002 (2002).

[2] V. Halyo *et al.*, Phys. Rev. Lett. **84**, 2576 (2000)

[3] E. R. Lee, *Microdrop Generation*, CRC Press, Boca Raton, (2002) ISBN 0-8493-1559-X

[4] D. Lebrun, C.E. Touil, and C. Özkul, Applied Optics **35**, 6375 (1996)

[5] Note that the measured density of the sample of Ultraol used differs significantly from the manufacturer's specification.

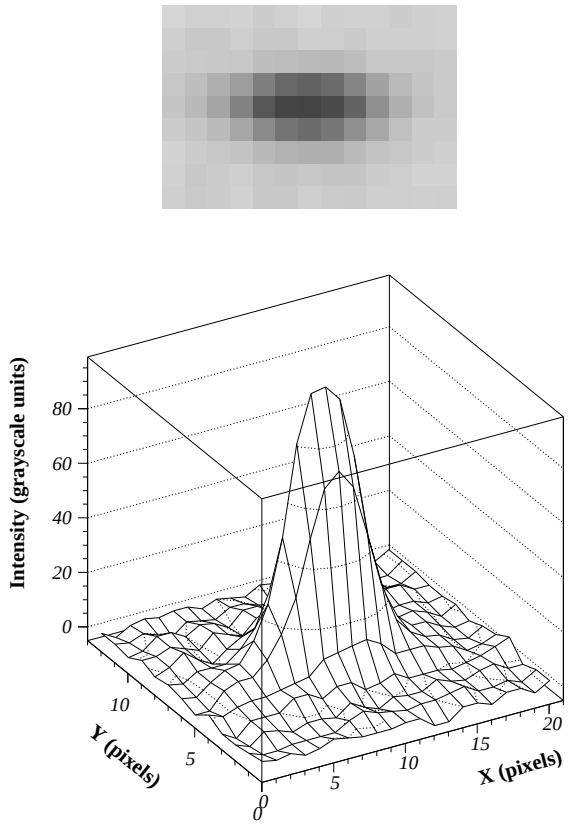

Figure 1: The image of a 20 μm diameter drop. The elliptical shape of the image is due to the aspect ratio of the effective pixels— the physical pixels are not square, and interlacing causes two adjacent pixels to be combined into one effective pixel.

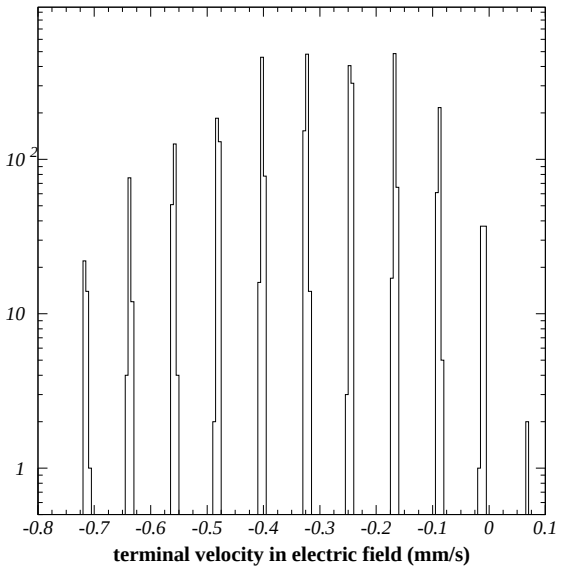

Figure 2: The observed peaks in the distribution of v_e, the terminal velocity in the presence of an electric field. Since the charge on each drop is quantized in units of e, the terminal velocity can only be certain discrete values.

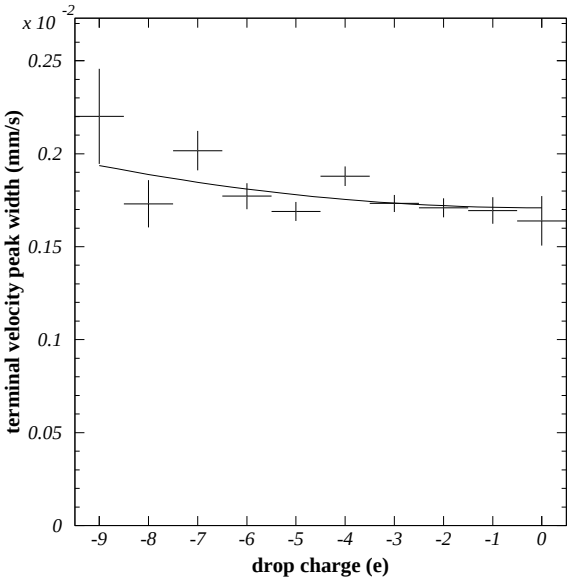

Figure 3: The measured peaks in the distribution of v_e have a width which increases as the absolute value of the charge increases. This increase can be used to determine the dispersion in the drop size.

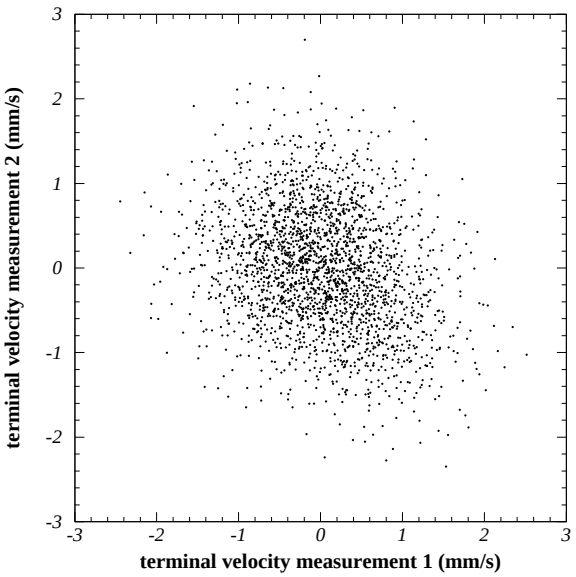

Figure 4: The anticorrelation between consecutive measurements, in data from 21.5 μm drops.

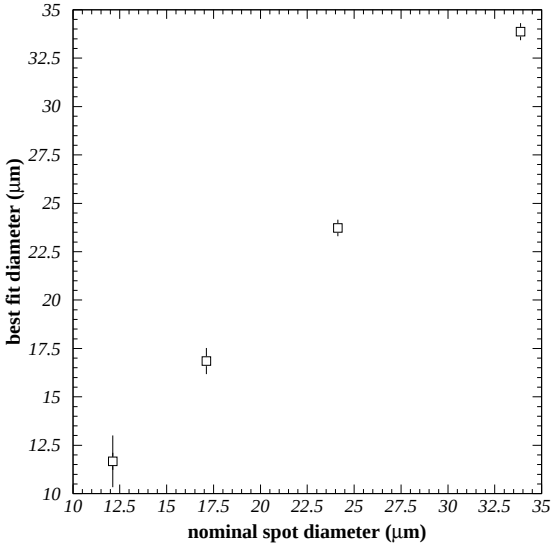

Figure 5: The best fit diameter ($2r$) for several simulated drop sizes. For clarity, the error bars are shown scaled by a factor of 3.

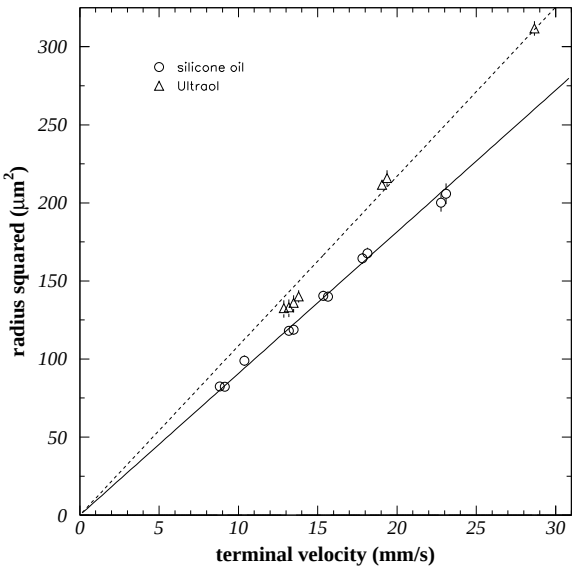

Figure 6: The apparent size (r^2, determined optically) as a function of the terminal velocity for a range of drop sizes, and two different fluids. The density of the fluids can be calculated from the slopes to be 0.94±0.02 g/cc for silicone oil, and 0.78±0.02 g/cc for Ultraol, in good agreement with direct measurement.